Impact of Interface Roughness Scattering on the Performance of $GaAs/Al_xGa_{1-x}As$ Terahertz Quantum Cascade Lasers

Yuri V. Flores and Asaf Albo

***Abstract*— We investigate the impact of interface roughness (IFR) scattering on the performance of a series of the state-of-the-art $GaAs/Al_xGa_{1-x}As$ terahertz quantum cascade lasers (THz-QCLs) through a calculation of the induced inhomogeneous broadening and intersubband scattering rates. Our analysis includes two $GaAs/Al_{0.15}Ga_{0.85}As$ THz-QCL devices with measured maximum operating temperatures at T_{max} = 177 K and 175 K, two $GaAs/Al_{0.30}Ga_{0.70}As$ devices with T_{max} = 150 K and 89 K, a $GaAs/AlAs\text{-}Al_{0.15}Ga_{0.85}As$ device with T_{max} = 181 K, and a GaAs/AlAs device that did not lase. The investigated QCL wafers were grown at the same solid-source molecular beam epitaxy facility and at fixed parameters, so that we expect a constant interface roughness quality for all devices. We find negligible impact of IFR scattering on the performance of devices that use $x = 0.15$ barriers as well as for devices that use $x = 0.30$ barriers with wide > 40 monolayers (ML) wells to support upper and lower laser levels. Fixing the barrier height to $x = 0.30$, we calculate a drastic increase of the IFR-induced linewidth broadening from ∼0.66 meV to ∼2 meV when the quantum wells thicknesses reduce from ∼40 ML to ∼30 ML and relate this effect to the observed reduction of T_{max} from 150 to 89 K. Furthermore, we calculate a large (∼2 meV) IFR linewidth broadening and short (∼1 ps) IFR intersubband scattering times for the device with pure AlAs layers and relate the consequent reduction of optical gain to the nonlasing of this device.**

***Index Terms*— Interface roughness, intersubband transitions, quantum cascade laser, terahertz emission.**

I. Introduction

THE crystal momentum for electrons confined in a two-dimensional semiconductor heterostructure can be split into a component parallel to the direction of epitaxial growth (k_z) and a component parallel to the heterostructure planes (k_{xy}). For perfectly smooth interfaces, k_{xy} is well defined due to the existing translational symmetry in the xy plane. In the more realistic case of rough interfaces, translational symmetry in the xy plane is broken, and, as a consequence, k_{xy} is not anymore clearly defined. Equivalently, the cross-plane (xy) quasi momentum conservation condition is relaxed due to the broken xy translational symmetry.

Interesting consequences of this effect have been reported on the performance of intersubband-lasers, whose working principle relies on stimulated photon emission between semiconductor conduction band states. Such devices, also known as quantum cascade lasers (QCLs), consist on alternated layers of typically 2–5 types of nanometer-thick III-V semiconductor compound materials with different energy bandgaps. By tailoring the layer thicknesses and through appropriate doping, one can engineer device parameters as the photon energy, oscillator strengths, and scattering rates. Using this approach–envisioned decades [1], [2] before its first demonstration in 1994 [3]– a wide range of QCL emission wavelengths has been reported, ranging from the mid-infrared (3–26 μm) to the far-infrared and terahertz (60–300 μm) regions of the electromagnetic spectrum. (For a review of research progress on QCLs we refer the interested reader to state of the art literature as for example Ref. [4].) The wide spectral range covered by QCLs makes these devices unique for a number of current and potential applications, including high-resolution spectroscopy, trace-gas sensing, local oscillators for heterodyne receivers, homeland security and biomedical imaging.

In QCLs, interface roughness (IFR) induces intrasubband and intersubband electron scattering [5]–[9]. Theoretical and experimental works [10]–[16] showed that IFR scattering plays an important role in the performance of mid-infrared QCLs. Examples are an induced linewidth broadening of $\sim 20-30$ meV [7], [13], a non-radiative scattering time between upper and lower laser level of $\sim 1-3$ ps [12], and large ($\sim 1-10$ kA/cm^2) shunt-type carrier leakage current into excited states [14]. Effects of IFR scattering are especially manifest in mid-infrared QCLs that use InGaAs/InAlAs alloys strain-compensated to InP [13], [14] due to the large (~ 1.5 eV) conduction band offsets (CBOs) used in the active region design. (As illustrated further down in section III, IFR scattering rates scale with the CBO squared).

In the THz-QCLs scientific community, on the other hand, only few research groups have reported works investigating the impact of IFR scattering on the laser performance [17]–[20]. A reason for this is that, historically, the low (∼0.135 eV) CBO compound semiconductor $GaAs/Al_{0.15}Ga_{0.85}As$ has served as standard material for realization of THz-QCLs. However, as the maximum

Manuscript received December 19, 2016; revised February 6, 2017, February 22, 2017, and March 11, 2017; accepted March 23, 2017. Date of publication March 30, 2017; date of current version April 25, 2017. The work of Y. V. Flores was supported by the Research Fellowship Program of the German Research Foundation, DFG, under Grant FL945/1-1. The work of A. Albo was supported in part by the MIT-Technion and the Andrew and Erna Finci Viterbi Fellowships as well as by the Bar-Ilan University Engineering Faculty Fellowship.

The authors are with the Research Laboratory of Electronics, Massachusetts Institute of Technology, Cambridge, MA 02139 USA (e-mail: yvf@mit.edu; asafalbo@gmail.com).

Color versions of one or more of the figures in this paper are available online at http://ieeexplore.ieee.org.

Digital Object Identifier 10.1109/JQE.2017.2689743

0018-9197 © 2017 IEEE. Personal use is permitted, but republication/redistribution requires IEEE permission.
See http://www.ieee.org/publications_standards/publications/rights/index.html for more information.

operating temperature of $GaAs/Al_{0.15}Ga_{0.85}As$-based THz-QCLs appears to converge towards the maximum reported value of ∼200 K [21], alternative material systems gain the attention of THz-QCL researchers including InGaAs/InGaAlAs [22], InGaAs/InAlAs [23], InGaAs/GaAsSb [24], and InAs/AlAsSb [25].

In addition to those material systems, the advantages of the $GaAs/Al_xGa_{1-x}As$ compound semiconductor with $x > 0.15$ have been explored for the realization of THz-QCLs with increased temperature insensitivity (e.g. in [26]–[31]). Key advantages of this material system are the induced isolation of active region states from the continuum states together with the possibility to fully suppress shunt-type electron leakage through excited states. The latter characteristic (suppression of shunt-type leakage) has been demonstrated very recently in [30] for a resonant-phonon $GaAs/Al_{0.30}Ga_{0.70}As$ THz-QCL via the measured negative differential resistance (NDR) over a wide $10 - 300$ K temperature range, which is a necessary condition to achieve stable lasing at such temperatures.

In [30], thin (∼28 monolayers (ML) thick) quantum wells and $Al_{0.30}Ga_{0.70}As$ barriers were used to increase the intersubband energy spacing between the upper laser level and the next excited state from ∼60 meV –a typical value in $GaAs/Al_{0.15}Ga_{0.85}As$ active region designs– up to ∼100 meV. Furthermore, although leakage into excited states was suppressed in that design, fabricated devices performed poorly, and it was speculated in [30] that increased IFR scattering might be responsible for the poor laser performance. Interestingly, a similar detriment of the laser performance was reported for so-called ground state $GaAs/Al_{0.30}Ga_{0.70}As$ THz-QCLs [27] when replacing the quantum well layer thicknesses by thinner values. The causes of such detriment were reported as unknown in [27].

In addition, inclusion of pure AlAs barriers has been suggested as alternative approach to reduce parasitic leakage currents [28]. However, as reported in [28], a design using pure AlAs barriers failed to lase and excessive IFR scattering triggered by the large CBO (∼1 eV) at the GaAs/AlAs interface was speculated to be the reason for this behavior. An interesting strategy to circumvent the sharp CBO discontinuity at the GaAs/AlAs interface is to use interface grading techniques as reported in [29], yet at the cost of using wide (∼55-97 ML) wells and, consequently, absent NDR.

In this work we follow a simple approach in order to quantify the impact of IFR scattering on the performance of state of the art $GaAs/Al_xGa_{1-x}As$ THz-QCLs. Investigated laser designs are the ones originally reported in [21], [28], [30] and [31], and we include in our analysis the THz-QCL design with the record maximum operating temperature of ∼200 K reported by Fathololoumi *et al.* in [21] as well as the THz-QCL design with thin wells that showed room-temperature NDR [30]. Using standard expressions for the IFR-induced inhomogeneous broadening and intersubband scattering rates, we analyze the interplay between CBOs and quantum well and barrier thicknesses in these devices and draw consequences for future design strategies.

The QCL samples discussed in this work were grown in the same solid source molecular beam epitaxy (MBE) growth facility (machine VB of Sandia Laboratories) and at fixed growth parameters (e.g. growth temperature of 630 °C), which is expected to lead to nearly the same IFR quality for all samples. As pointed out in [32], researchers need to be careful when comparing the performance of lasers from different laboratories/growth sources. By using samples from the same facility we reduce the risk of over- or underestimation of key quantities (e.g. doping, layer thickness fluctuations, roughness parameters) within a particular set of wafers, and increase the confidence of the analysis' conclusions.

We find that a combination of high ($x = 0.30$) barriers and thin (∼30 ML thick) wells in the active region design leads to a drastic increase of the linewidth broadening up to ∼ 2 meV, considerably affecting the laser performance. We further find that IFR-induced shunt-type electron leakage into higher states might become relevant for highly-doped ($>10^{11}$ cm^{-2}) devices that use large Al compositions in the barriers. Furthermore, in devices with pure AlAs barriers, IFR-induced intersubband scattering from the upper into the lower laser level might be fast enough to considerably reduce the upper laser level lifetime, affecting laser performance further.

II. Investigated Lasers

The investigated THz-QCLs are presented in Fig. 1 together with relevant design parameters. The structures are two $GaAs/Al_{0.15}Ga_{0.85}As$ designs (A, Fig. 1a and B, Fig. 1b), two $GaAs/Al_{0.30}Ga_{0.70}As$ designs (C, Fig. 1c and D, Fig. 1d), a $GaAs/AlAs\text{-}Al_{0.15}Ga_{0.85}As$ design (E, Fig. 1e) and a GaAs/AlAs design (F, Fig. 1f). The designs use a three quantum well (one well injector) active region and are based on the resonant phonon extraction scheme.

Device A is a standard diagonal THz-QCL design with maximum operating temperature $T_{max} = 177$ K [30], [31]. Device B is a regrowth of the THz-QCL design with the record maximum operating temperature of ∼200 K [21]. The regrowth design showed $T_{max} = 175$ K [28]. Device D ($T_{max} = 89$ K [30]) achieves the same wavelength alignment than device C ($T_{max} = 150$ K [30]) yet it uses thinner wells in order increase the intersubband energy spacing between the upper laser level and next excited state to ∼100 meV and –opposite to device C– it shows room temperature NDR [30]. Device E ($T_{max} = 181$ K [28]) emulates the wavelength alignment of device B yet the injector barrier of device B is replaced by pure AlAs. Device F uses pure AlAs barriers in the active region design and did not lase [28].

For calculations we use a CBO of 0.135 eV [33] for the $GaAs/Al_{0.15}Ga_{0.85}As$ heterointerface, 0.259 eV [34] for the $GaAs/Al_{0.30}Ga_{0.70}As$ and 1.05 eV [28] for the GaAs/AlAs heterointerface. We calculate wavefunctions and eigenenergies using a 3-band Schrödinger equation solver as outlined in [35]. The THz-QCL designs were processed into metal-metal ridges as reported in the original references, leading to a nearly unity optical confinement factor in the direction perpendicular to the heterostructure planes [33]. Further details on the laser structures and performance parameters are presented in Tab. I.

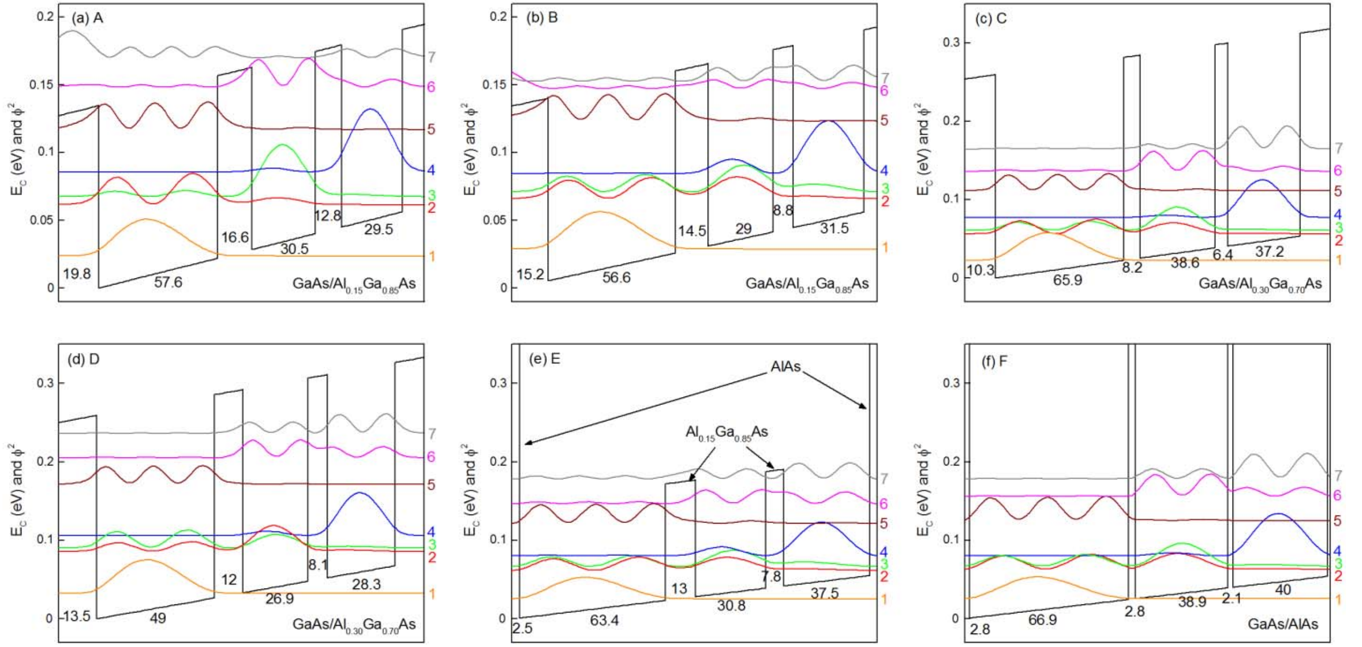

Fig. 1. Conduction band profile (1 module) at design bias for the investigated THz-QCLs. Relevant wavefunctions and layer thicknesses (in monolayers) are indicated.

TABLE I

DEVICE PARAMETERS AND PERFORMANCE

Device	Wafer/Ref.	x in Al$_x$Ga$_{1-x}$As	E_{43} (THz)	f_{43}	z_{43} (nm)	n_s (cm^{-2})	$J_{th}(T_l)$ (A/cm^2)	$J_{max}(T_l)$ (A/cm^2)	$\Delta J(T_l)$ (A/cm^2)	T_{max} (K)
A	VB0605 [30][31]	0.15	4.00	0.17	0.63	6×10^{10}	246 (10 K)	825 (10 K)	579 (10 K)	177
B	VB0486 [28][a]	0.15	3.26	0.56	1.26	3×10^{10}	1150 (10 K)	1400 (10 K)	250 (10 K)	175
C	VB0676 [30]	0.30	3.95	0.18	0.65	6×10^{10}	457 (10 K)	851 (10 K)	394 (10 K)	150
D	VB0743 [30]	0.30	3.78	0.16	0.62	6×10^{10}	725 (10 K)	897 (10 K)	172 (10 K)	89
E	VB0487 [28]	1.0-0.15[b]	3.30	0.54	1.23	3×10^{10}	1110 (76 K)	1400 (76 K)	290 (76 K)	181
F	VB0548 [28]	1.0	3.16	0.16	0.68	1.2×10^{11}	–	–	–	–

Indicated are, from left to right, the device name, wafer number and original reference, Al composition, designed central emission frequency, oscillator strength, dipole matrix element, sheet density per period (all samples are doped in the middle (4.8 nm) of the widest well), threshold current density for the given lattice temperature T_l, maximum current density, dynamic range and maximum operating temperature. These laser performance parameters were measured for ($\sim$2 mm $\times$ 150 μm) ridges in pulsed operation mode at a low (0.02 %) duty cycle. The active region thicknesses were in all cases $\sim$10 μm.

[a]The active region design for device B was originally reported in [21]. This design was then regrown in the same MBE machine as the other devices investigated in this work. The regrown device was reported in [28].

[b]Device E uses the GaAs/Al$_{0.15}$Ga$_{0.85}$As material system yet with pure AlAs injector barriers (Fig. 1e).

III. CALCULATION RESULTS

Table II summarizes calculated scattering times for IFR-induced intersubband scattering between selected states. These values are obtained assuming a Gaussian auto-correlation function of the roughness $\langle h(\vec{r})h(\vec{r}')\rangle = \Delta^2 \exp(-|\vec{r}-\vec{r}'|/\Lambda^2)$ with an average in-depth roughness height Δ and an in-plane ($\vec{r}$) correlation length Λ as [12]:

$$\frac{1}{\tau_{m,n}^{IFR}} = \frac{\pi m_c}{\hbar^3}\Delta^2\Lambda^2\sum_i \delta U_i^2 \varphi_m^2(z_i)\varphi_n^2(z_i)\exp\left(\frac{-\Lambda^2 q_{mn}^2}{4}\right), \tag{1}$$

where $m_c = 0.067 m_0$ is the effective mass for conduction band electrons in the quantum well material, $\varphi_{m,n}(z_i)$ are the wavefunction amplitudes of states m, n at the ith interface, and q_{mn} is the two-dimensional scattering vector involved in the scattering process. Assuming parabolic bands, $\hbar q_{mn} = \sqrt{2m_c E_{mn}}$ with the intersubband energy spacing $E_{mn} = |E_m - E_n|$ between levels m, n. Similarly, the IFR-induced inhomogeneous broadening between subbands m and n is calculated as [10], [11]:

$$\Gamma_{m,n}^{IFR} = \frac{\pi m_c}{\hbar^2}\Delta^2\Lambda^2\sum_i \delta U_i^2\left(\varphi_m^2(z_i) - \varphi_n^2(z_i)\right)^2. \tag{2}$$

TABLE II
CALCULATION RESULTS

Device	$\tau_{4,3}^{IFR}$ (ps)	$\tau_{4,3}^{LO}$ (ps)	$\tau_{2,1}^{IFR}$ (ps)	$\tau_{2,5}^{IFR}$ (ps)	$\tau_{2,6}^{IFR}$ (ps)	$\tau_{2,7}^{IFR}$ (ps)	$\tau_{3,5}^{IFR}$ (ps)	$\tau_{3,6}^{IFR}$ (ps)	$\tau_{3,7}^{IFR}$ (ps)	$\tau_{4,5}^{IFR}$ (ps)	$\tau_{4,6}^{IFR}$ (ps)	$\tau_{4,7}^{IFR}$ (ps)	$\Gamma_{4,3}^{IFR}$ (meV)	T_2^{*IFR} (ps)
A	12.43	1.9	11.1	2.94	15.76	—[a]	12.63	3.35	—[a]	155.3	6.48	9.11	0.84	1.83
B	6.86	0.42	14.53	4.09	15.04	5.1	2.37	26.75	8.03	38.25	10.2	8.09	0.34	25.4
C	8.41	2.1	9.44	2.52	4.45	17.39	5.13	2.87	14.48	49.97	3.22	2.22	0.66	1.56
D	5.71	1.8	6.51	2.39	2.14	6.01	1.61	3.90	11.05	57.32	1.79	2.29	2.04	1.07
E	5.17	0.44	7.07	1.32	1.64	2.12	0.91	1.99	2.01	15.0	2.11	4.23	0.70	1.35
F	1.22	1.4	3.89	0.54	0.72	2.37	1.14	0.58	2.65	9.24	0.50	0.78	2.10	2.59

[a] $\tau_{2,7}^{IFR}$ and $\tau_{3,7}^{IFR}$ are omitted for structure A due to the unbound nature of state 7 in this design.

For our calculations we use $\Delta = 1$ Å and $\Lambda = 6$ nm as measured for an InGaAs/InAlAs-based QCL active region [36]. Although the roughness parameters' values are still matter of debate in the QCL scientific community (see for example [8]), we consider that the used values for (Δ, Λ) are realistic (see also discussion in III. D.). For a discussion on different interface roughness models in QCLs we refer the interested reader to the work of Franckié *et al.* [20]. Further discussions on the impact of different values of (Δ, Λ) on the resulting IFR scattering rates in QCLs can be found in [8], [9].

We draw several conclusions from Tab. II and summarize them as follows:

A. IFR Intersubband Scattering From the Upper Into the Lower Laser Level ($\tau_{4,3}^{IFR}$)

With exception of device F, calculated $\tau_{4,3}^{\mathrm{IFR}}$ values remain much larger than typical non-radiative scattering times for scattering from the upper into the lower laser level via LO-phonon emission ($\tau_{4,3}^{\mathrm{LO}} \sim 0.5 - 2$ ps, as indicated in Tab. II). For a fixed barrier height (device A vs. device B), we find reduced $\tau_{4,3}^{\mathrm{IFR}}$ values for devices with larger oscillator strengths due to the increased wavefunctions overlap. Similarly, in devices with similar oscillator strength (A vs. C) $\tau_{4,3}^{\mathrm{IFR}}$ is reduced by ~30 % from 12.43 ps to 8.41 ps when the Al composition increased from 0.15 to 0.30.

For device F we calculate $\tau_{4,3}^{\mathrm{IFR}} = 1.22$ ps as a result of the much higher CBOs (pure AlAs barriers). This short time lies close to the lifetime for LO-phonon emission for this design ($\tau_{4,3}^{\mathrm{IFR}} = 1.4$ ps). As a result, the effective upper laser level lifetime reduces by a factor of ~ 2 due to the action of IFR scattering. As we explain further down, this short lifetime contributes to the bad performance (non lasing) of this device.

B. IFR Intersubband Scattering From the Lower Laser Level Into the Injector State ($\tau_{2,1}^{IFR}$)

IFR-induced scattering from electron from level 2 into level 1 remains in all cases negligibly small compared to electron LO-phonon emission ($\tau_{2,1}^{\mathrm{LO}} \sim 0.2 - 0.3$ ps for all investigated devices due to resonant-phonon extraction design). This is mainly related to the ground state nature of level 1, which decays very fast at the barriers, leading to small values of $\varphi_2^2 \varphi_1^2$ (Eq. 1) at the interfaces of the widest quantum well. Larger CBOs lead to smaller values for $\tau_{2,1}^{\mathrm{IFR}}$, yet the absolute values remain large compared to LO-phonon emission rates.

C. Shunt-Type Electron Leakage Into Excited States ($\tau_{m,n}^{IFR}$, With $m = 2, 3, 4$ and $n = 5, 6, 7$)

IFR-induced shunt-type carrier leakage current into excited states is defined as intersubband scattering from QCL active region states into excited states. This type of leakage current depends on the portion of electrons in the initial subband with enough energy to scatter elastically into the final subband and is therefore strongly temperature-dependent.

Using the calculated raw scattering times in Tab. II we estimate the magnitude of the shunt-type leakage current for electrons escaping from the upper laser level 4 into excited states 5, 6 and 7. As outlined in detail in [14], [37], this is done assuming thermally distributed subbands and weighting the raw scattering times $\tau_{4,5}^{IFR}$, $\tau_{4,6}^{IFR}$ and $\tau_{4,7}^{IFR}$ ps with the portion of electrons in level 4 available to scatter elastically into levels 5, 6 and 7 ([37, Eq. 10]). The population of level 4 has to be known for this calculation and we use here an estimated steady-state value of $n_4 = 0.3 n_s$ [38]. Fig. 2 shows calculated values for shunt-type leakage $J_{4,5}^{IFR} + J_{4,6}^{IFR} + J_{4,7}^{IFR}$ for the different THz-QCL designs as a function of electron temperature for subband 4, $T_{e,4}$. We consider for the calculations $T_{e,4}$ values within $100 - 300$ K. This range of subband electron temperatures corresponds to lattice temperatures between $T_l \sim 10{-}300$ K. As shown in [35], [39], $T_{e,4}$ is ~100 K for $T_l \sim 10 - 80$ K and, at higher lattice temperatures, $T_{e,4}$ converges to T_l due to the efficient cooling of electrons via LO-phonon scattering.

We see in Fig. 2 that only low shunt-type electron leakage current values are found for the large majority of investigated samples. We categorize the found values as low as they represent only a small part of the total current density at threshold ($J_{th} \sim 0.3 - 1.5$ kA/cm^2 for $T_l \sim 10 - 200$ K). An exception here is the design that incorporates pure AlAs barriers in the active region. Large CBOs in this design lead to short raw times $\tau_{4,(5,6,7)}^{\mathrm{IFR}}$. However, averaged over the subband

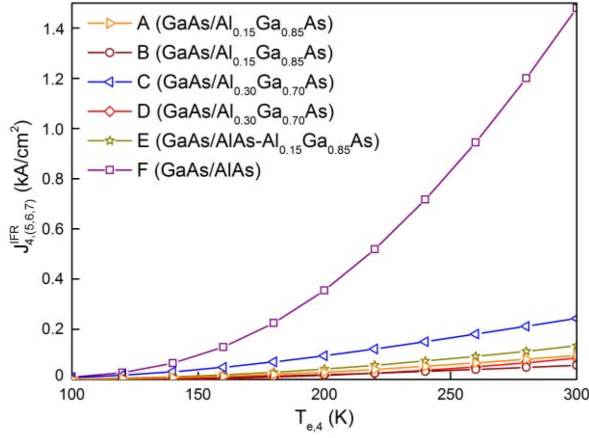

Fig. 2. Calculated shunt-type leakage current density for electrons escaping from the upper laser level 4 into levels 5, 6 and 7 via intersubband IFR scattering. We use for calculations a subband population for level 4 of $n_4 = 0.3n_s$, with n_s values as indicated in Tab. I.

distribution, they lead to negligibly small values of $J^{\mathrm{IFR}}_{4,(5,6,7)}$ for temperatures up to $T_{e,4} \sim 150$ K. For larger temperatures we calculate relatively large values of $J^{\mathrm{IFR}}_{4,(5,6,7)}$ for design F as a consequence of the low $\tau^{\mathrm{IFR}}_{4,(5,6,7)}$ values together with the high-doping used in this device (Tab. I). Design F did not show lasing even at a temperature of 10 K, so it is rather difficult to correlate the calculated leakage currents to the device performance. However, our calculation shows that IFR-induced shunt-type leakage from the upper laser level into excited states might become relevant for highly-doped THz-QCL designs that incorporate pure AlAs barriers.

Interestingly, the calculated scattering times for shunt-type electron leakage from levels 2 and 3 into excited states are comparable or lower to the values calculated for leakage out of level 4 (see for example calculated values for E and F in Tab. II). The use of high doping was recently suggested as a strategy to compensate the loss of optical gain in highly-diagonal ($f_{4,3} \sim 0.2$) devices [40]. Such devices would experience a fast depopulation of levels 2 and 3 as a consequence of a large leakage current $J^{IFR}_{2,(5,6,7)}$ and $J^{IFR}_{3,(5,6,7)}$ triggered not only by the relatively short scattering times but also by the larger electron temperature in these levels compared to the electron temperature of level 4 [35], [39]. Very recently the authors showed in [38] how this kind of leakage current can effectively counteract the population inversion decrease that arises from the remaining non-radiative scattering channels as the temperature increases, contributing positively to the laser performance.

D. Linewidth Broadening ($\Gamma^{IFR}_{4,3}$)

The calculated IFR-induced linewidth broadening values for the investigated THz-QCL structures lie within $0.66 - 2.10$ meV. These values are close to the ones obtained by Schrottke *et al.* [41] when fitting experimental slope efficiency vs. current density data in THz-QCLs. The authors in [41] obtained $\gamma_0 = 0.5 - 1$ meV, where γ_0 is a broadening free parameter that describes interface roughness ([41, Eq. 2 and Fig. 3]).

IFR-induced linewidth broadening in addition to the inherent lifetime broadening of the upper and lower laser levels ($\sim$1 meV each) will approximate the total linewidth broadening. The last has been experimentally estimated to be $\sim$4 meV from electroluminescence [42] and recently also from time-domain spectroscopy measurements [43], [44]. Note that works (e.g. [45]) have been reported that use $\Delta = 2.825$ Å (1 monolayer, ML) and $\Lambda = 10$ nm as roughness parameters for modeling GaAs/$Al_{0.15}Ga_{0.85}$As THz-QCLs. However, following Eq. 2, such a pair of (Δ, Λ) would lead to overestimated values for the linewidth broadening ($\sim 10 - 40$ meV for the structures investigated in this work).

Because of the arguments raised above, we consider that the values obtained in this work for the IFR-induced broadening as well as for the IFR-induced intersubband scattering rates are realistic. In the following we discuss in more detail the obtained IFR linewidth broadening values for the different THz-QCL structures.

A comparison between structures A ($\Gamma^{IFR}_{4,3} = 0.84$ meV) and B (0.34 meV) –both with $Al_{0.15}Ga_{0.85}$As barriers– shows that the IFR linewidth broadening is reduced by almost a factor of ~ 2 in the "more vertical" design B ($z^B_{43} = 1.26$ nm vs. $z^A_{43} = 0.63$ nm) due to smaller contributions of $\varphi^2_4 - \varphi^2_3$ at each interface (Eq. 2). Similarly, in design C (which resembles design A yet using $Al_{0.30}Ga_{0.70}$As barriers) we calculate a somewhat smaller IFR linewidth broadening (0.66 meV) than for device A. From Eq. 2 we see that this is because the increased scattering potential at the interfaces in device C is compensated by a much faster decaying term $\left(\varphi^2_4 - \varphi^2_3\right)^2$.

In addition, a comparison between devices B ($\Gamma^{IFR}_{4,3} = 0.34$ meV) and E (0.70 meV) –which have almost identical wavefunction alignment [28]– shows that the inclusion of pure AlAs injector barriers resulted in a doubled linewidth broadening. This effect is a consequence of the interplay of high CBO at the injector/upper-laser-level-quantum-well interface and the induced wavefunctions penetration at this interface.

In order to illustrate the effect of narrower quantum wells on the linewidth broadening we plot in Fig. 3 the contributions of individual interfaces to the total IFR-induced linewidth broadening in designs C and D. These designs have almost identical wavefunctions alignment yet design D uses narrower quantum wells in order to "push" excited states towards higher eigenenergies [30]. As a result, device D showed negative differential resistance at room temperature yet also a larger threshold current density than device C (Tab. I).

Fig. 3 shows that the narrow wells in device D lead to larger penetration of the wavefunctions at the interfaces and, as a consequence, to larger contributions of each interface to the total linewidth broadening. Summing over all interfaces (Eq. 2) we calculate a IFR-induced linewidth broadening of 2.04 meV for device D vs. a value of 0.64 for device C. We relate this significant increase of the linewidth broadening and consequent reduction of the laser gain to the poorer performance of device D ($T_{max} = 89$ K for device D vs. $T_{max} = 150$ K for device C), although virtual suppression of carrier leakage into higher states was achieved in device D by pushing excited

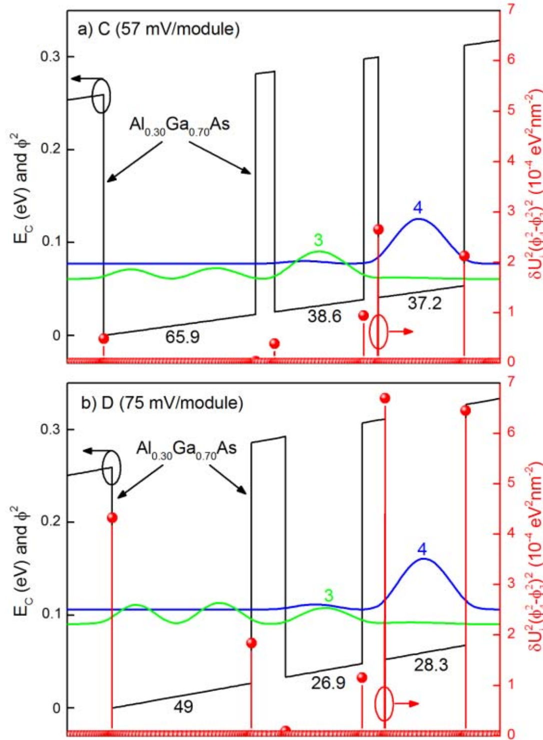

Fig. 3. Illustration of the impact of individual interfaces on the IFR-induced linewidth broadening between upper (4) and lower (3) laser states for design C (a) and D (b). The term $\delta U_i^2 \left(\varphi_4^2(z_i) - \varphi_3^2(z_i)\right)^2$ of Eq. 2 is represented with red dots.

states towards higher eigenenergies [30]. This effect also explains why ground state THz-QCLs [27] –which use narrow wells in order to push excited states into higher energies– perform poorly compared to standard resonant phonon designs. The same effect leads also to device degradation within ground state THz-QCLs (e.g. the $GaAs/Al_{0.30}Ga_{0.70}As$ ground state THz-QCL structure in [27] performed poorly (structure TWIGS254, $T_{max} = 24$ K) compared to a similar structure yet with wider wells (structure OWIGS271, $T_{max} = 71$ K), although excited states in structure TWIGS254 were pushed towards higher eigenenergies.)

Furthermore, a relatively large (2.10 meV) IFR linewidth broadening is calculated for device F as a consequence of the inclusion of pure AlAs barriers in the active region design. Following the arguments raised above we attribute the bad performance (non-lasing) of this device to a combination of: 1) the increased IFR linewidth broadening, 2) the short upper laser level lifetime (section III. A.) due to IFR intersubband scattering from the upper into the lower laser level, 3) the low oscillator strength, and 4) a probable increase of the optical loss due to the high doping in this device.

E. Pure Dephasing Time Due to IFR Intrasubband Scattering (T_2^{*IFR})

Finally, it is important to mention that IFR scattering induces incoherent resonant tunneling in QCLs, damping the Rabi oscillations of the electron wave packet across the injector barrier. This can be understood as a series of destructive interferences of the wave packet's frequencies induced by the fluctuations of the injector barrier width and height [46]. Such effect is described by a dephasing time $\tau_{4,inj}^{deph}$ as $\frac{1}{\tau_{4,inj}^{deph}} = \frac{1}{2\tau_4} + \frac{1}{2\tau_{inj}} + \frac{1}{T_2^*}$ [9]. τ_4 and τ_{inj} are due to all intersubband scattering processes that involve the upper laser level 4 and the injector level from the previous cascade, inj (not shown in Fig. 1). T_2^* is due to all intrasubband scattering mechanisms that cause energy broadening of states 4 and inj and is referred in the literature as "pure dephasing time". We calculate the dephasing time due to IFR intrasubband scattering as $T_2^{*IFR} = \hbar/\Gamma_{4,inj}^{IFR}$ and include the results in Tab. II ($\Gamma_{4,inj}^{IFR}$ is calculated using Eq. 2). The obtained values for T_2^{*IFR} lie within $T_2^{*IFR} = 1.07-25.4$ ps. Note that phenomenological values $T_2^* \sim 0.3-0.6$ ps are used in THz-QCL transport simulations (e.g. in [35], [47]–[50]) and that those times are much shorter than the calculated T_2^{*IFR}. This means that additional subband broadening mechanisms besides IFR contribute significantly to the pure dephasing time including intrasubband electron-electron scattering, ionized impurities, and alloy disorder scattering. (For a detailed discussion on the impact of specific intra- and intersubband scattering mechanisms on the dephasing times we refer the interested reader to the work of Terazzi [51].) Altogether we find that inclusion of additional intra- and intersubband scattering mechanisms besides IFR is necessary for an extended analysis of the impact of dephasing on the performance of specific THz-QCL designs.

IV. Conclusion

In conclusion, we discussed the impact of interface roughness (IFR)-induced intrasubband and intersubband scattering on the performance of state of the art $GaAs/Al_xGa_{1-x}As$ THz-QCLs. We pointed out to warning regions in the parameter space for THz-QCL design, where the effects of IFR scattering become critical for the laser performance. Examples of those regions are the inclusion of pure AlAs barriers in the active region design as well as the usage of $Al_{0.30}Ga_{0.70}As$ barriers with thin ($<$30 monolayers) quantum wells to support the laser states. Simultaneously, quantum wells thinner than 35 monolayers are necessary to suppress thermally activated leakage into excited states. The latter rule is crucial for QCL performance as it leads to negative differential resistance over a wide 10 − 300 K temperature range, which is a necessary condition to achieve stable lasing at such temperatures. These findings should assist semiconductor device engineers to cultivate novel design strategies towards room-temperature terahertz light-emitting semiconductor lasers.

V. Acknowledgment

The authors gratefully acknowledge Prof. Qing Hu for the devoted mentoring, the many enlightening discussions and for the generous support in performing this research. The authors thank valuable discussions with Prof. Dan Botez on the topic of interface roughness scattering. The authors further thank John L. Reno for the MBE growths. A. A. acknowledges the generosity and support of the MIT-Technion and the Andrew and Erna Finci Viterbi Fellowships as well as of the

Bar-Ilan University Engineering Faculty Fellowship. Y. V. F. acknowledges the support of the Research Fellowship Program of the German Research Foundation, DFG (Grant FL945/1-1).

REFERENCES

[1] R. F. Kazarinov and R. A. Suris, “Possibility of amplification of electromagnetic waves in a semiconductor with a superlattice,” *Semicond. Phys. Technol.*, vol. 5, p. 797, Oct. 1971.
[2] F. Capasso, “Band-gap engineering: From physics and materials to new semiconductor devices,” *Science*, vol. 235, p. 172, Jan. 1987.
[3] J. Faist, F. Capasso, D. L. Sivco, C. Sirtori, A. L. Hutchinson, and Y. A. Cho, “Quantum cascade laser,” *Science*, vol. 264, no. 5158, p. 553, 1994.
[4] M. S. Vitiello, G. Scalari, B. Williams, and P. De Natale, “Quantum cascade lasers: 20 years of challenges,” *Opt. Exp.*, vol. 23, no. 4, p. 5167, 2015.
[5] S.-C. Lee and A. Wacker, “Nonequilibrium Green’s function theory for transport and gain properties of quantum cascade structures,” *Phys. Rev. B, Condens. Matter*, vol. 66, no. 24, p. 245314, 2002.
[6] J. B. Khurgin, “Inhomogeneous origin of the interface roughness broadening of intersubband transitions,” *Appl. Phys. Lett.*, vol. 93, no. 9, p. 091104, 2008.
[7] A. Wittmann, Y. Bonetti, J. Faist, E. Gini, and M. Giovannini, “Intersubband linewidths in quantum cascade laser designs,” *Appl. Phys. Lett.*, vol. 93, no. 14, p. 141103, 2008.
[8] J. B. Khurgin and Y. Dikmelik, “Multiple roles of interface roughness scattering in QCL,” presented at the Intersubband Transitions Quantum Wells (ITQW), Montreal, QC, Canada, Sep. 2009.
[9] J. Faist, *Quantum Cascade Lasers*. Oxford, U.K.: Oxford Univ. Press, 2013.
[10] J. B. Khurgin *et al.*, “Role of interface roughness in the transport and lasing characteristics of quantum-cascade lasers,” *Appl. Phys. Lett.*, vol. 94, no. 9, p. 091101, 2009.
[11] A. Bismuto, R. Terazzi, M. Beck, and J. Faist, “Influence of the growth temperature of the performances of strain-balanced quantum cascade lasers,” *Appl. Phys. Lett.*, vol. 98, no. 9, p. 091105, 2011.
[12] Y. T. Chiu, Y. Dikmelik, P. Q. Liu, N. L. Aung, J. B. Khurgin, and C. F. Gmachl, “Importance of interface roughness induced intersubband scattering in mid-infrared quantum cascade lasers,” *Appl. Phys. Lett.*, vol. 101, no. 17, p. 171117, 2012.
[13] M. P. Semtsiv, Y. Flores, M. Chashnikova, G. Monastyrskyi, and W. T. Masselink, “Low-threshold intersubband laser based on interface-scattering-rate engineering,” *Appl. Phys. Lett.*, vol. 100, no. 16, p. 163502, 2012.
[14] Y. V. Flores, S. S. Kurlov, M. Elagin, M. P. Semtsiv, and W. T. Masselink, “Leakage current in quantum-cascade lasers through interface roughness scattering,” *Appl. Phys. Lett.*, vol. 103, no. 16, p. 161102, 2013.
[15] D. Botez, C.-C. Chang, and L. J. Mawst, “Temperature sensitivity of the electro-optical characteristics for mid-infrared (λ = 3-16 μm)-emitting quantum cascade lasers,” *J. Phys. D, Appl. Phys.*, vol. 49, p. 43001, 2016.
[16] S. Mathonnière, M. P. Semtsiv, and W. T. Masselink, “Thermal annealing of lattice-matched InGaAs/InAlAs quantum-cascade lasers,” *J. Cryst. Growth*, to be published. [Online]. Available: http://dx.doi.org/10.1016/j.jcrysgro.2017.01.029
[17] S. G. Razavipour, E. Dupont, Z. R. Wasilewski, and D. Ban, “Effects of interface roughness scattering on device performance of indirectly pumped terahertz quantum cascade lasers,” *J. Phys., Conf. Ser.*, vol. 619, no. 1, p. 012003, 2015.
[18] C. Deutsch *et al.*, “Probing scattering mechanisms with symmetric quantum cascade lasers,” *Opt. Exp.*, vol. 21, no. 6, p. 7209, 2013.
[19] K. A. Krivas, D. O. Winge, M. Franckié, and A. Wacker, “Influence of interface roughness in quantum cascade lasers,” *J. Appl. Phys.*, vol. 118, no. 11, p. 114501, 2015.
[20] M. Franckié *et al.*, “Impact of interface roughness distributions on the operation of quantum cascade lasers,” *Opt. Exp.*, vol. 23, no. 4, p. 5201, 2015.
[21] S. Fathololoumi *et al.*, “Terahertz quantum cascade lasers operating to 200 K with optimized oscillator strength and improved injection tunneling,” *Opt. Exp.*, vol. 4, no. 4, p. 3866, 2012.
[22] K. Ohtani, M. Beck, and J. Faist, “Strain-compensated InGaAs terahertz quantum cascade lasers,” *ACS Phot.*, vol. 3, no. 12, p. 2297, 2016.
[23] C. Deutsch *et al.*, “High power growth-robust InGaAs/InAlAs terahertz quantum cascade lasers,” *ACS Phot.*, to be published, [Online]. Available: http://pubs.acs.org/doi/abs/10.1021/acsphotonics.7b00009
[24] C. Deutsch *et al.*, “High performance InGaAs/GaAsSb terahertz quantum cascade lasers operating up to 142 K,” *Appl. Phys. Lett.*, vol. 101, no. 21, p. 211117, 2012.
[25] M. Brandstetter *et al.*, “InAs based terahertz quantum cascade lasers,” *Appl. Phys. Lett.*, vol. 108, no. 1, p. 011109, 2016.
[26] E. Dupont *et al.*, “A phonon scattering assisted injection and extraction based terahertz quantum cascade laser,” *J. Appl. Phys.*, vol. 111, no. 7, p. 073111, 2012.
[27] C. W. I. Chan, Q. Hu, and L. J. Reno, “Ground state terahertz quantum cascade lasers,” *Appl. Phys. Lett.*, vol. 101, no. 15, p. 151108, 2012.
[28] C. W. I. Chan, Q. Hu, and L. J. Reno, “Tall-barrier terahertz quantum cascade lasers,” *Appl. Phys. Lett.*, vol. 103, no. 15, p. 151117, 2013.
[29] L. Schrottke, X. Lü, G. Rozas, K. Biermann, and H. T. Grahn, “Terahertz GaAs/AlAs quantum-cascade lasers,” *Appl. Phys. Lett.*, vol. 108, no. 10, p. 102102, 2016.
[30] A. Albo, Q. Hu, and J. L. Reno, “Room temperature negative differential resistance in terahertz quantum cascade laser structures,” *Appl. Phys. Lett.*, vol. 109, no. 8, p. 081102, 2016.
[31] A. Albo and Q. Hu, “Carrier leakage into the continuum in diagonal GaAs/$Al_{0.15}$GaAs terahertz quantum cascade lasers,” *Appl. Phys. Lett.*, vol. 107, no. 24, p. 241101, 2015.
[32] D. O. Winge, M. Franckié, and A. Wacker, “Simulating terahertz quantum cascade lasers: Trends from samples from different labs,” *J. Appl. Phys.*, vol. 120, no. 11, p. 114302, 2016.
[33] B. S. Williams, “Terahertz quantum cascade lasers,” Ph.D. dissertation, Dept. Elect. Eng. Comput. Sci., Massachusetts Inst. Technol., Cambridge, MA, USA, 2003.
[34] I. Vurgaftman, J. R. Meyer, and L. R. Ram-Mohan, “Band parameters for III–V compound semiconductors and their alloys,” *J. Appl. Phys.*, vol. 89, no. 11, p. 5815, 2001.
[35] C. W. I. Chan, “Towards room-temperature terahertz quantum cascade lasers: Directions and design,” Ph.D. dissertation, Dept. Elect. Eng. Comput. Sci., Massachusetts Inst. Technol., Cambridge, MA, USA, 2015.
[36] P. Offermans, P. M. Koenraad, J. H. Wolter, M. Beck, T. Aellen, and J. Faist, “Digital alloy interface grading of an InAlAs/InGaAs quantum cascade laser structure studied by cross-sectional scanning tunneling microscopy,” *Appl. Phys. Lett.*, vol. 83, no. 20, p. 4131, 2003.
[37] Y. V. Flores, S. S. Kurlov, M. Elagin, M. P. Semtsiv, and W. T. Masselink, “The role of electron temperature in the leakage current in QCLs and its impact on the quantum efficiency,” in *Proc. SPIE 9002, Novel In-Plane Semiconductor Lasers XIII*, San Francisco, CA, USA, 2014, Art. no. 90021R, doi: 10.1117/12.2036371.
[38] A. Albo and Y. V. Flores, “Temperature-driven enhancement of the stimulated emission rate in terahertz quantum cascade lasers,” *IEEE J. Quant. Elect.*, vol. 53, no. 1, Feb. 2017, Art. no. 2300105.
[39] A. Albo and Q. Hu, “Investigating temperature degradation in THz quantum cascade lasers by examination of temperature dependence of output power,” *Appl. Phys. Lett.*, vol. 106, no. 13, p. 131108, 2015.
[40] C. W. I. Chan, A. Albo, Q. Hu, and J. L. Reno, “Tradeoffs between oscillator strength and lifetime in terahertz quantum cascade lasers,” *Appl. Phys. Lett.*, vol. 109, no. 20, p. 201104, 2016.
[41] L. Schrottke, M. Wienold, M. Giehler, R. Hey, and H. T. Grahn, “Analysis of the slope efficiency for terahertz quantum-cascade lasers,” *Appl. Phys. Lett.*, vol. 108, no. 10, p. 103108, 2010.
[42] B. S. Williams, H. Callebaut, S. Kumar, and Q. Hu, “3.4-THz quantum cascade laser based on longitudinal-optical-phonon scattering for depopulation,” *Appl. Phys. Lett.*, vol. 82, no. 7, p. 1015, 2003.
[43] D. Burghoff, T.-Y. Kao, D. Ban, A. W. M. Lee, Q. Hu, and J. Reno, “A terahertz pulse emitter monolithically integrated with a quantum cascade laser,” *Appl. Phys. Lett.*, vol. 98, no. 6, p. 061112, 2011.
[44] D. P. Burghoff, “Broadband terahertz photonics,” Ph.D. dissertation, Dept. Elect. Eng. Comput. Sci., Massachusetts Inst. Technol., Cambridge, MA, USA, 2014.
[45] H. Callebaut, “Analysis of the electron transport properties in quantum cascade lasers,” Ph.D. dissertation, Dept. Elect. Eng. Comput. Sci., Massachusetts Inst. Technol., Cambridge, MA, USA, 2006.
[46] F. Eickemeyer *et al.*, “Ultrafast coherent electron transport in semiconductor quantum cascade structures,” *Phys. Rev. Lett.*, vol. 89, no. 4, p. 047402, 2002.
[47] S. Kumar and Q. Hu, “Coherence of resonant-tunneling transport in terahertz quantum-cascade lasers,” *Phys. Rev. B, Condens. Matter*, vol. 80, no. 24, p. 245316, 2009.
[48] H. Callebaut and Q. Hu, “Importance of coherence for electron transport in terahertz quantum cascade lasers,” *J. Appl. Phys.*, vol. 98, no. 10, p. 104505, 2005.

[49] E. Dupont, S. Fathololoumi, and H. C. Liu, "Simplified density-matrix model applied to three-well terahertz quantum cascade lasers," *Phys. Rev. B, Condens. Matter*, vol. 81, no. 20, p. 205311, 2010.

[50] P. Tzenov, D. Burghoff, Q. Hu, and C. Jirauschek, "Time domain modeling of terahertz quantum cascade lasers for frequency comb generation," *Opt. Exp.*, vol. 24, no. 20, p. 23232, 2016.

[51] R. L. Terazzi, "Transport in quantum cascade lasers," Ph.D. dissertation, Dept. Phys., ETH Zürich, Zürich, Switzerland, 2012.

Yuri V. Flores was born in Baku, Azerbaijan, in 1986. He received the B.Sc. degree from the Leibniz University of Hannover, Hannover, Germany, in 2010, and the M.Sc. degree and the Ph.D. degree (Highest Hons.) from the Humboldt University Berlin, Germany, in 2013 and 2015, respectively, all in physics. He gained research experience at the Institute of Transport- and Automation Technology, Hannover, where he developed software tools for RFID applications and at the Ferdinand-Braun-Institute, Berlin, where we conducted characterization studies on (Al,In,Ga)N ultraviolet LDs and LEDs. His research at Humboldt University focused on the development of a realistic model for the description of electron transport in mid-infrared (Al,In,Ga)As quantum cascade lasers (QCLs) strain-balanced to InP, which led to the development of novel scientific approaches to investigate temperature-driven carrier leakage phenomena. He has authored or co-authored 23 technical papers and is currently a Post-Doctoral Research Fellow with the Research Laboratory of Electronics, Massachusetts Institute of Technology, where he studies the carrier dynamics in terahertz QCLs and develops novel design strategies for high-performance terahertz light-emitting semiconductor lasers.

Asaf Albo received the B.Sc. degrees (Hons.) in physics and materials engineering from the Technion, Israel Institute of the Technology in 2002, the M.Sc. degree from the Department of Materials Engineering, Technion, Israel Institute of the Technology, in 2005, and the Ph.D. degree from the Department of Electrical Engineering, Technion, Israel Institute of the Technology, in 2011. He was a Research and Development Senior Physicist in the semiconductor industry for four years (2010–2013). He is currently a Research Associate with the Research Laboratory of Electronics, Massachusetts Institute of Technology, where he studies the carrier dynamics in terahertz quantum cascade lasers and develops novel design strategies for high-performance intersubband lasers for terahertz light emission. He is also a Materials and Devices Researcher that specializes in semiconductors, quantum-structures and their optoelectronic devices. Dr. Albo will be leading a new established Research Group at the Faculty of Engineering at Bar-Ilan University, Israel.